Study on the Simultaneous Control of the Seam Tracking and Leg Length in a Horizontal Fillet Welding
Part 1: Analysis and Measurement of the Weld Bead Geometry

H. S. Moon and S. J. Na

Abstract

Among the various welding conditions, the welding current that is inversely proportional to the tip-to-work-piece distance is an essential parameter as to monitor the GMAW process and to implement the welding automation. Considering the weld pool surface geometry including weld defects, it should modify the signal processing method for automatic seam tracking in horizontal fillet welding. To meet the above necessities, a mathematical model related with the weld pool geometry was proposed as in a conjunction with the two-dimensional heat flow analysis of the horizontal fillet welding. The signal processing method based on the artificial neural network (Adaptive Resonance Theory) was proposed for discriminating the sound weld pool surface from that with the weld defects. The reliability of the numerical model and the signal processing method proposed were evaluated through the experiments of which showed that they are effective for predicting the weld bead shape with or without the weld defects in a horizontal fillet welding.

Key Words : Horizontal fillet welding, Weld bead shape, Numerical analysis, Current measurement, Neural network

1. Introduction

Various kinds of forces that act on the weld pool surface are classified into three groups: gravitational force, force due to the arc pressure, and surface tension force. In spite of the important role of a weld bead geometry in the weld quality, the works pertaining to the weld bead geometry have not yet been studied in depth.

A number of investigators have studied the magnitude of the arc pressure in gas tungsten arc welding(GTAW) as well as the weld pool geometry affected by the arc pressure and gravitational force. In the previous works on the weld pool geometry in arc welding[1,2,3], it was assumed that the dominant factor in the formation of weld bead shape was the gravity of while the arc pressure was considered to be negligibly small. However, these works could not explain or predict the formation of the weld defects such as the undercut, overlap, or excess convexity.

H. S. Moon is with the Industrial Research Institute, Hyundai Heavy Industry Co. Ltd., Ulsan, Korea.

S. J. Na is a Professor in Department of Mechanical Engineering, Korea Advanced Institute of Science and Technology, Taejon, Korea

E-mail : sjna@kaist.ac.kr, Tel : +82-42-869-3216

Among the various welding parameters, the welding current that is inversely proportional to the tip-to-work-piece distance in the GMAW is an essential parameter needed to monitor the GMAW process of the horizontal fillet joints and to implement the automatic seam tracking by using arc sensors [4,5,6,7,8]. An adequate signal-processing algorithm is indispensable for improving the performance of the arc sensors thereby.

In this paper, a mathematical model related with the pool surface geometry in the horizontal fillet welding was proposed in conjunction with a two-dimensional heat flow analysis to predict the weld bead shape and weld defects. Moreover, a signal processing method based on the artificial neural network was proposed for discriminating the current signal of sound weld beads from that of weld beads with overlap.

2. Governing equation of weld pool surface

The main weld defects occurring in the horizontal fillet welding are the undercut, overlap, and excess convexity. The typical cross-sectional shapes of the sound weld bead and of that with the weld defects mentioned above are shown in Fig. 1. In order to achieve a satisfactory weld bead geometry without the weld defects, it is

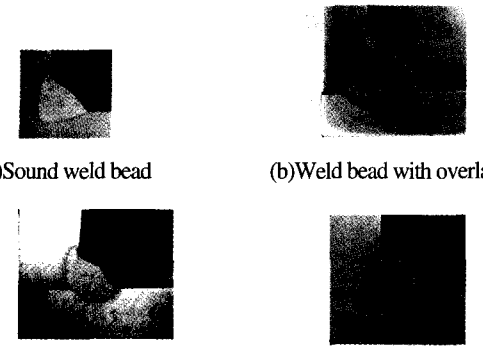

(a)Sound weld bead (b)Weld bead with overlap

(c)Weld bead with undercut (d)Weld bead with excess convexity

Fig. 1 Typical weld bead shapes

necessary to study the effect of the welding conditions affecting the weld bead geometry, and also the tendency of weld defects in various welding conditions.

Figure 2 shows the coordinates system used in the model. The surface equation defined as z(x, y) should have two solutions in the undercut and overlap area, which makes it impossible to predict these defects. To overcome the above drawback, the bead shape was assumed to change along the x-axis, so that the surface equation was defined as x(y, z) in this paper. Let x(y, z) be the surface equation at a position (y, z) under the assumption that the surface deviates only slightly from an original value. The area A_s shown in Fig. 3 stands for the deformed surface area, and is given approximately as follows.

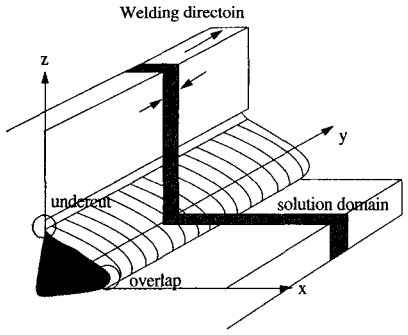

Fig. 2 Solution domain and coordinates used in model

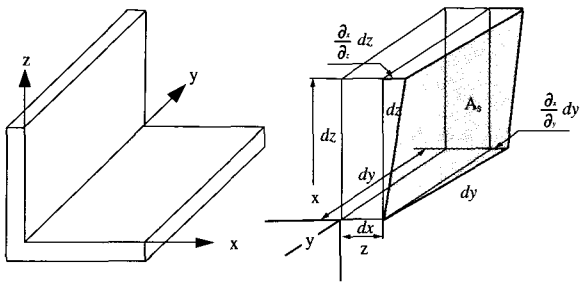

Fig. 3 Surface variation of weld pool

$$A_s=\iint_s dy'dx'=\iint_s\sqrt{1+(\frac{\partial x}{\partial y})^2+(\frac{\partial x}{\partial z})^2+(\frac{\partial x}{\partial y})^2(\frac{\partial x}{\partial z})^2}dydz$$
$$\approx\iint_s\sqrt{1+(\frac{\partial x}{\partial y})^2+(\frac{\partial x}{\partial z})^2}\,dydz \quad (1)$$

A surface depression will form a shape that minimizes the total energy. Hence a calculus of variation may be used to determine the weld bead shape under the action of gravitational force, arc pressure and surface tension. The surface shape is subject to the constraint that the volume of weld bead is the same as that of the wire fed into the weld pool. In this model, it was assumed that there was no convection in the molten pool to simplify the mathematical model [9]. The energy to be minimized is the potential energy in the gravitational field and the work performed by arc pressure and surface energy. The total energy acting on the infinitesimal area A_s, E is given as follows [10].

$$E=\iint_s(\sigma\sqrt{1+(\frac{\partial x}{\partial y})^2+(\frac{\partial x}{\partial z})^2}+\rho gzx+P_a)dydz\equiv\iint_s Fdydz \quad (2)$$

Of where σ are the surface tension, ρ the density for steel and p_a the arc pressure. In this study, σ was assumed to be constant because there is only a negligible difference as the result of temperature variation [11].

The additional volume of electrode wire fed into the weld joint is regarded as a constraint condition and is given as follows.

$$\iint_s xdydz\equiv\iint_s Gdydz=\frac{\pi r^2 f}{V_w}=\frac{\pi r^2\alpha I}{V_w} \quad (3)$$

Of where r is the radius of the electrode wire, f the wire feed rate, α the mapping factor between the wire feed rate and welding current, *Vw and I the welding current* the welding speed.

The necessary condition for the solution follows from application of the appropriate Eular equation.

$$\frac{\partial}{\partial y}\{\frac{\partial x}{\partial xy}(F+\lambda G)\}+\frac{\partial}{\partial z}\{\frac{\partial}{\partial xz}(F+\lambda G)\}-\frac{\partial}{\partial x}(F+\lambda G)=0 \quad (4)$$

Of where λ is the Lagrange multiplier.

From the above Euler equation, the following equation can be derived, if the variation of bead shape in the y-axis direction is supposed to be zero.

$$\sigma\left[\frac{\chi_{zz}}{(1+\chi_z^2)^{3/2}}\right]=\rho gz+P_a+\lambda \quad (5)$$

The arc pressure P_a with a Gaussian distribution was adopted from the reference[1]. The material properties used in this model are : ρ =7200 kg/m^3, g =9.8m/sec^2, σ =1.2N/m. To determine the Lagrange multiplier λ, the golden section search was used [12].

3. Heat transfer in horizontal fillet welding

The magnitude of the melting zones across the x- and z-axis should be determined to solve the equation (5). The hatched area shown in Fig. 2 is the solution domain for heat flow and surface shape of weld pools. The end effects resulting from either the initiation or termination of the heat source in the solution domain are neglected. Then, the heat transfer problem that has the three-dimensional character can be reduced to a two-dimensional unsteady temperature field at a section normal to the weld line. The two-dimensional unsteady heat transfer equation is expressed as follows.

$$\frac{\partial}{\partial x}\left(k\frac{\partial T}{\partial x}\right)+\frac{\partial}{\partial z}\left(k\frac{\partial T}{\partial z}\right)=\rho C_p\frac{\partial T}{\partial t} \quad (6)$$

Of where k is the thermal conductivity, ρ the density, C_p the specific heat, T the temperature.

A Gaussian distribution that can be expressed in the following equation specified the heat flux from arc to the work-piece.

$$q(r)=\frac{3Q}{\pi \bar{r}^2}\exp\{-3(r/\bar{r})^2\} \quad (7)$$

Of where $q(r)$ is the heat flux at the radial distance r from the arc center, $\bar{r}$ the effective radius of arc and Q the power transferred into the weldment.

A fully implicit method was used to differentiate the time, and the control volume formulation was used to derive the discrete equations, which were solved by using a TDMA(Tri-diagonal-Matrix Algorithm) [13].

Selection of the appropriate meshes is indispensable to the acceptable accuracy of the finite difference results and the small computing time required. The more severe the temperature gradient is in a region, the more nodes are required. Thus, a grid mesh with the variable spacing that is very fine near the heat source and increases gradually away from it, has had been used[14].

Before the center of the heat source passes the solution domain, the heat flux is assumed to be located on the base metal. In this analysis step, the area of filler metal in the domain is considered to have the physical properties of the air. After the joint is filled with the filler metal, the heat flux is treated to be located on the weld pool which possesses now the physical properties of filler metal.

4. Simulation results and discussion

The solving procedure for determining the surface profile of the weld pool is shown concisely in the flowchart of Fig. 4, where the melting zone is determined by the heat transfer analysis and the surface profile by the equation (5). Figure 5 shows the fusion boundaries and weld bead surface profiles resulting from the mathematical model just after the heat flux passes the solution domain and the experimental results obtained under various welding conditions.

In Fig. 5(a), the welding current(wire feed rate) was relatively high compared with other welding conditions, while the welding speed was adequate to compensate for it. Consequently the results of the mathematical model and experiment show a good agreement for the weld bead shape and no weld defects in appearance. In Fig. 5(b), the welding current was relatively high compared with other welding conditions, while the welding speed was too low, which caused the overlap both in calculated and experimental bead shape. It is well known that the higher the welding current and the lower the welding speed, the greater the susceptibility to overlap. This is due to the fact that the large weld pool flows downward due to the gravitational force, while its wetting is blocked by the surface tension between the liquid and solid surface. A relatively large discrepancy was found between the experimental and calculated fusion zone size of base metal. It is probably due to the fact that, the large weld pool prohibits the arc heat from conducting into the base metal of while in the calculation, the weld bead is generated only after the center of the heat source passes the solution domain. In Fig. 5(c), it can be shown that the undercut occurred under the condition of low welding

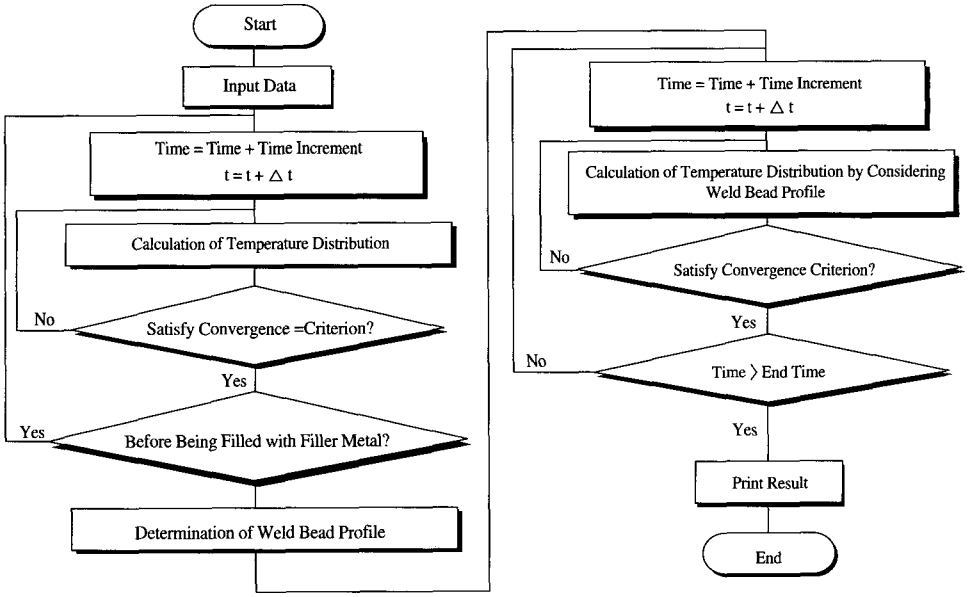

Fig. 4 Flow chart for calculation of temperature distribution and weld pool shape

current and high welding speed. The main cause of undercut is that the welding arc cuts into the base metal, while the cut area cannot be filled with filler metal because of a high welding speed. In Fig. 5(d), the welding speed was relatively high compared with the welding current, while the latter was not too low, which resulted in a weld bead with excess convexity. It is probably due to the rapid cooling of weld pool edges. These results show that the proposed model can fairly well predict the weld defects such as undercut, overlap and excess convexity caused by an improper combination of process parameters in horizontal fillet welding. Although the welding conditions used in this modeling is different from these of the following section and Part2 of this paper, the results of the weld pool model were used to select initial welding conditions which may not cause the overlap during seam tracking.

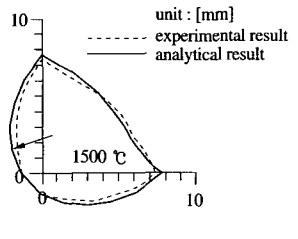

(a) Sound weld bead
(wire feed rate(f) = 9.4(m/min),
arc voltage(V) = 28(V),
welding speed(V_w) = 6(mm/sec))

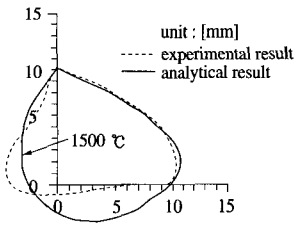

(b) Bead with overlap
(wire feed rate(f)=9.1(m/min),
arc voltage(V)=30(V)
welding speed(V_w)=4(mm/sec))

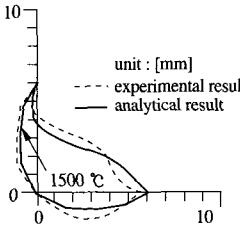

(c) Bead with undercut
(with feed rate(f)=6.4(m/min),
arc voltage(V)=26(V),
welding speed(V_w)=8(mm/sec)

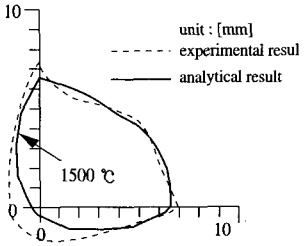

(d) Bead with excess convexity
(wire feed rate(f)=6.9(m/min),
arc voltage(V)=26(V),
welding speed(V_w)=7(mm/sec))

Fig. 5 Comparison of experimental and calculated bead shapes

5. Recognition of overlap by current measurement

5.1 Adaptive resonance theory (ART2)

The adaptive Resonance architecture has a characteristic of stable self-organized classification in response to the arbitrary sequence of the input patterns. The basic principles of adaptive resonance theory were introduced by Grossberg[15]. A class of the adaptive resonance architectures, called ART, has since been characterized as a system of ordinary differential equations by Carpenter and Grossberg. This theorem predicts both of the order of search, as a function of the learning history of the network, and the asymptotic category structure self-organized by arbitrary sequences of binary input patterns.

ART2 accepts analog (or gray-scale) vector components as well as binary components, which contributes to a significant enhancement of the system [15,16,17]. The overall structure of the ART2 network is shown in Figure 6. The F1 layer has been divided into six sub-layers, w, x, u, v, p, and q. Each node labeled G is a gain control unit that sends a nonspecific inhibitory signal to each unit on the layer. All sub-layers on F1, as well as the r layer of the orienting subsystem, have the same number units. Individual sub-layers on F1 are connected unit to unit; that is, the layers are not fully interconnected, with the exception of the bottom-up connections to F2 and the top-down connections from F2. The F1 layer includes several processing levels and gain control system. The bottom-up input patterns and the top-down signals are received at each different locations in the F1. A positive feedback loops within F1 enhances the salient features and suppresses the noise. The basic algorithm is as follows. If the input vector(welding current signals) does not match with any stored patterns, a new category is created by storing the current input vector. Once a stored pattern is found to match with the input vector within a classification criterion, that pattern is adjusted to be the same as the input vector. No stored pattern is ever modified, if it does not match with the current input pattern within the given vigilance. In this way, the stability-plasticity dilemma is overcome, that is , new pattern can create some additional classification categories, but a new input pattern cannot cause the existing memory to be changed unless they match closely.

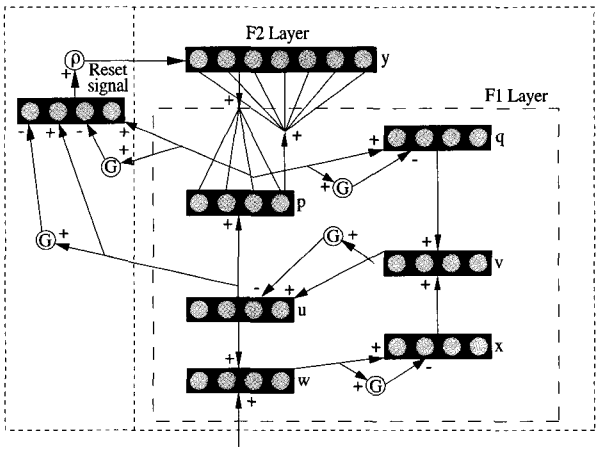

Fig. 6 Overall structure of the ART2 network

5.2 Implementation of ART2 to pattern classification

To examine the characteristics of each welding current signal, a series of experiments were carried out under the various welding conditions. The welding current signal was measured when the welding torch was oscillated within the groove. To enhance the reliability of the measured signal, the digital low pass filter with a cutoff frequency of 10 Hz was used, while the sampling rate was 1 kHz. The robot torch moves from left to right for the first weaving and from right to left for the second weaving, which repeats up to the end of welding.

The typical signal patterns can be classified into two types, that is, for the weld bead with and without overlap. Figures 7(a) and 7(b) show the representative welding current waveforms measured for the following welding conditions.

The waveforms of the welding current signal measured during horizontal fillet welding show a U-shape for every weaving motion, because the weld pool is influenced by the molten pool motion and arc pressure and tends to have a round shape. The welding current signal of Fig. 7(a) for the weld pool without overlap is expected to be a symmetric curve, while the signal of Fig. 7(b) measured for the weld pool with overlap is basically different from the symmetric waveform. The waveform of Fig. 7(b) shows a somewhat flat shape because of the overlap caused by the gravitational force which induces the

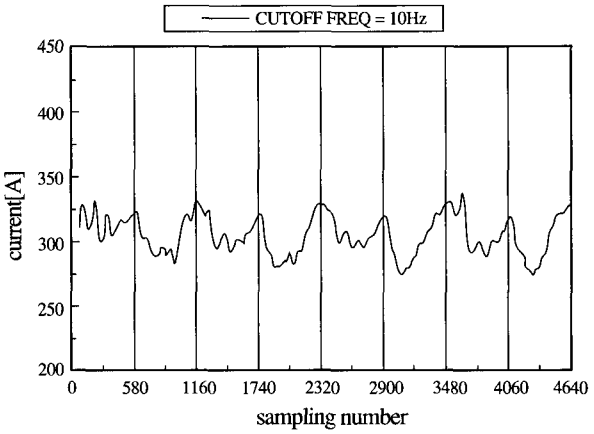

(a) Weld pool without overlap

(f = 10.9[m/min], V = 32[V], V_w = 6[mm/sec], offset distance = 0[mm], weaving time = 0.6[sec], dwell time=0.3[sec], weaving length = 10[mm], shielding gas : Ar 80% + CO_2 20%)

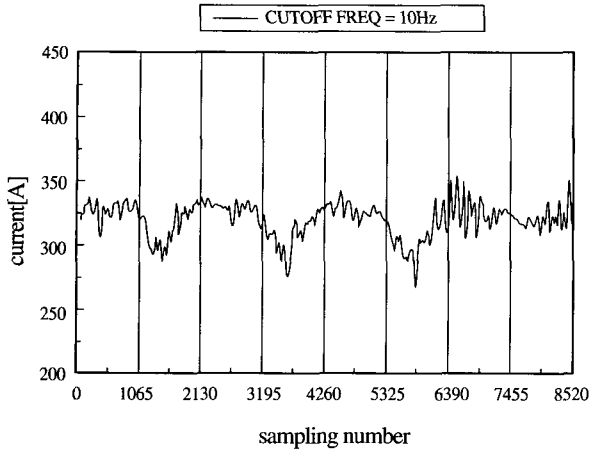

(b) Weld pool with overlap

(f = 10.9[m/min], V = 32[V], V_w = 4[mm/sec], offset distance = 0[mm], weaving time = 1[sec], dwell time = 0.3[sec], weaving length = 10[mm], shielding gas : Ar 80% + CO_2 20%)

Fig. 7 Typical waveforms of current signal

deposited molten metal to fall downward. Consequently the variation of tip-to-work-piece distance experienced during torch motion from left to right is smaller than the value of the case without overlap.

When the center of torch is shifted to left or right with a offset distance of 2mm as depicted in Fig. 8, the waveform is dramatically changed. In this case, when the torch is moved closely to left end or right end of weaving, the welding current signal shows a high value because of a very small tip-to-work-piece distance. However, when the center of torch is shifted to left or right with a offset distance, the leg ratio(L1/L2) turned out to be very small or very large. The very small (or very large) leg length ratio finally results in bad weld qualities. Figures 9(a) and 9(b) show the welding current waveforms measured for the following welding conditions.

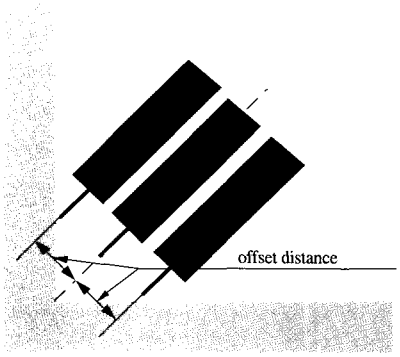

Fig. 8 Definition of offset distance

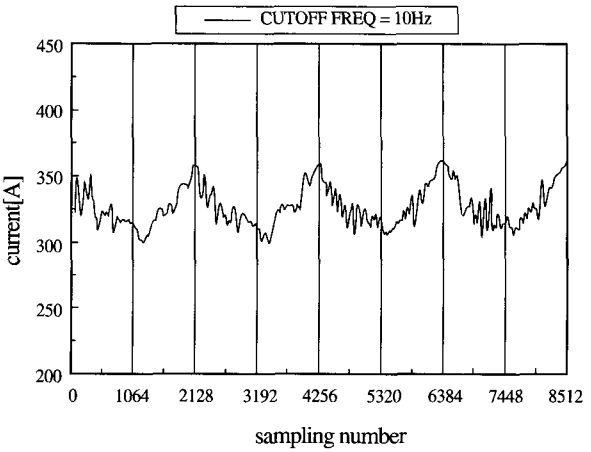

(a) Center of torch is shifted to left

(f = 10.9[m/min], V = 32[V], V_w = 6[mm/sec], offset distance = 2[mm] at left, weaving time = 1[sec], dwell time=0.15[sec], weaving length = 8[mm])

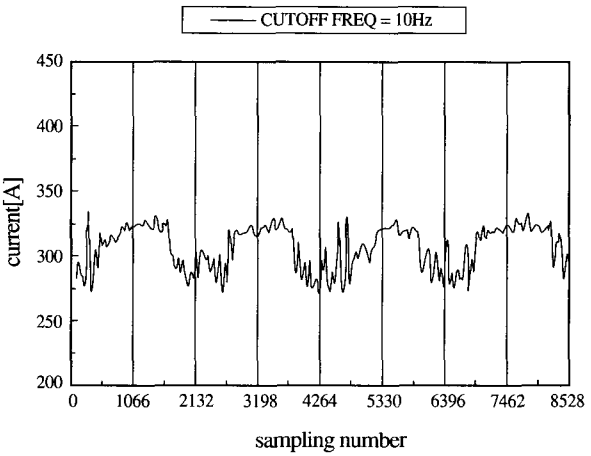

(b) Center of torch is shifted to left

(f = 10.9[m/min], V = 32[V], V_w = 6[mm/sec], offset distance = 2[mm] at right, weaving time = 1[sec], dwell time = 0.15[sec], weaving length = 8[mm])

Fig. 9 Typical waveforms of current signal

Based on the above results, the pattern classification algorithm was implemented by using ART2 to decide whether the overlap occurred or not. The input patterns used in the ART2 pattern-matching process consist of various waveforms as well as the two representative waveforms mentioned above. Figure 10 shows the results of the pattern classification determined by the ART2 matching process. From these results, it can be insisted that the occurrence of overlap can be predicted by measuring the welding current signal during the weaving motion and ART2 pattern classification described in Section 5.1 and Section 5.2. In part 2 of this paper, this

signal processing algorithm will be adopted to determine whether welding conditions bring about the overlap or not during seam tracking.

6. Conclusion

It is extremely complicated to find out the effect of the welding process parameters on the weld quality for the characteristics of the welding process are the highly non-linear and heavily complex. Due to the above drawbacks, the two-dimensional heat transfer analysis and mathematical model of the weld pool surface profile were adopted to overcome the time consuming experiments needed to select the appropriate welding conditions in the horizontal fillet welding. The weld bead profiles predicted by the model were examined through various experiments. Weld defects such as overlap, undercut and excess convexity could be effectively estimated by the proposed mathematical model. Moreover, the ART2 network was implemented to classify the weld bead shape with or without overlap by measuring the welding current signal during every

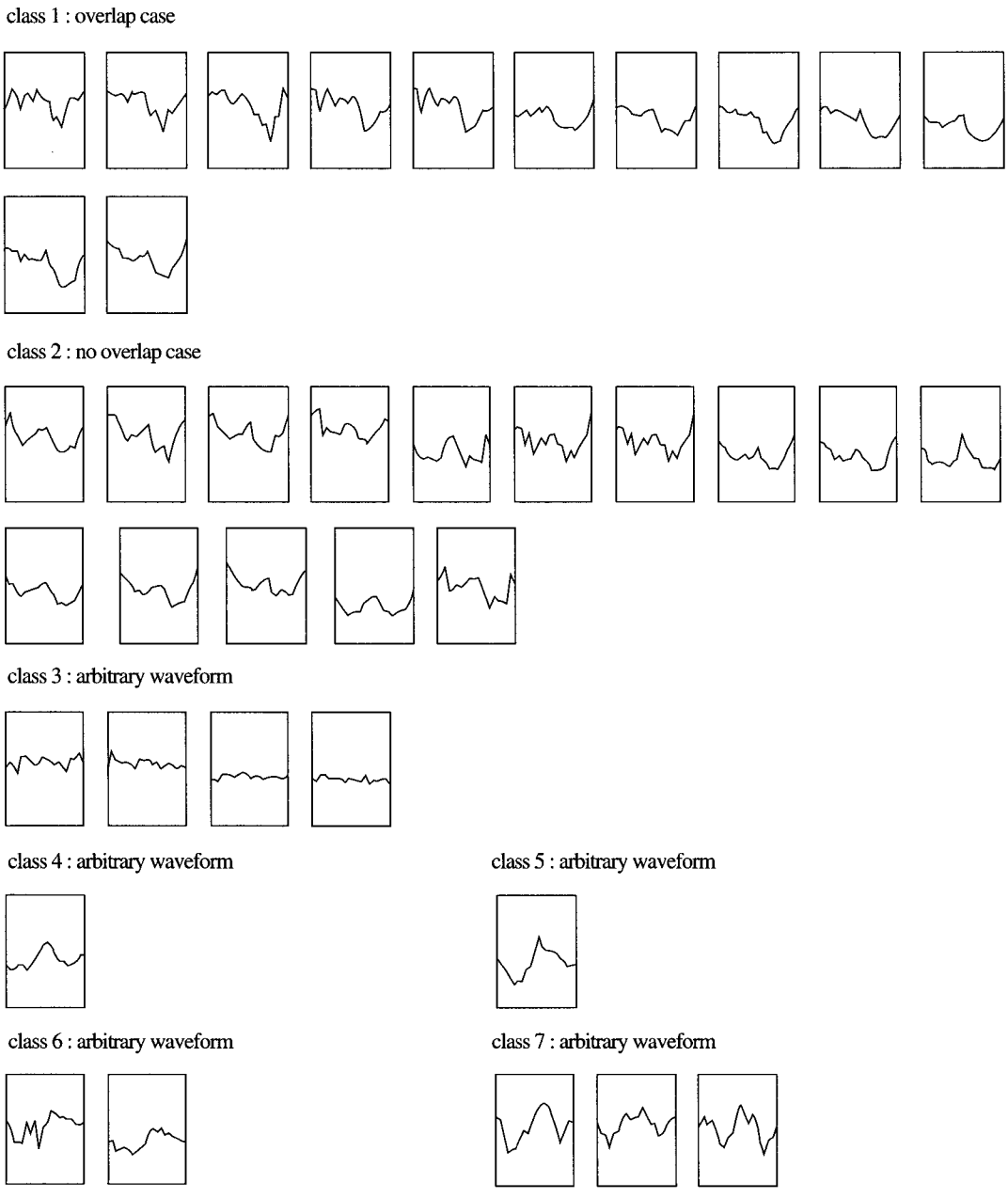

Fig. 10 Results of pattern classification by using ART2

weaving. It was found that the waveform of the welding current signal could be used to determine whether the weld defect of overlap occurred in horizontal fillet welding or not. This algorithm can also be used for the quality control of the weldments in a conjunction with the automatic seam tracking.

References

1. L. Lin and T. W. Eagar: Influence of Arc Pressure on Weld Pool Geometry, Research Supplement, *Welding Journal,* Vol. 64, No. 6 (1985), pp.163s-169s
2. K. Nishiguchi, T. Ohji and H. Matsui: Fundamental Researches on Bead Formation in Overlaying and Fillet Welding Processes, *Journal of the Japan Welding Society,* Vol. 45, No. 1 (1976), pp.82-87
3. K. Nishiguchi, T. Ohji and Y. Yoshida: A Nonlinear Model of Molten Pool in Arc Welding, *Journal of the Japan Welding Society,* Vol. 4, No. 4 (1986), pp.19-23
4. H. Nomura and Y. Sugitani: Development of Automatic Fillet Welding Process with High Speed Rotating Arc, *Nippon Kokan Technical Report,* Vol. 47 (1986), pp.65-71
5. H. Nomura, Y. Sugitani and Y. Suzuki: Automatic Real-time Bead Height Control with Arc Sensor in TIG Welding, *Transactions of the Japan Welding Society,* Vol.18, No. 2 (1987), pp.125-132
6. H. Fujimura, E. Ide and H. Inoue: Joint Tracking Control Sensor of GMAW-Development of Method and Equipment for Position Sensing in Welding with Electric Arc Signals (Report 1), *Transactions of the Japan Welding Society,* Vol. 18, No. 1 (1987), pp.32-40
7. M. Ushio: Sensor in Arc Welding, *Transactions of Japan Welding Research Institute,* Vol. 20, No. 2 (1991), pp.157-163
8. J. W. Kim and S. J. Na: A study on Arc Sensor Algorithm for Weld Seam Tracking in Gas Metal Arc Welding of Butt Joints, *Proc. Instn. Mech. Engrs. Part B : Journ. of Engng. Manufacture,* Vol. 205 (1991), pp.247-255
9. T. Zacharia, A. H. Eraslan and D. K. Aidun: Modeling of Non-Autogenous Welding, Research Supplement, *Welding Journal,* Vol. 67, No. 1 (1988), pp.18s- 27s
10. L. D. Landau and E. M. Lifshitz: Fluid Mechanics, *Pergamon Press,* (1959)
11. J. W. Kim and S. J. Na: A Study on the Three-Dimensional Analysis of Heat and Fluid Flow in Gas Metal Arc Welding Using Boundary-Fitted Coordinates, *Proc. Instn. Mech. Engrs. Part B : Journal of Engng. Manufacture,* Vol. 206 (1992), pp.159-173
12. J. J. Arora: Introduction to Optimum Design, *McGraw-Hill Book Company,* (1989), pp.295-300
13. S. V. Patankar: Numerical Heat Transfer and Fluid Flow, *McGraw-Hill Book Company,* (1980), pp.64-68
14. T. J. Lho and S. J. Na: A Study on Three-Dimensional Transient Heat Flow in Circumferential GTA Welding of Pipe Using Periodicity Conditions, *Proc. Instn. Mech. Engrs., Part B : Journal of Engng. Manufacture,* Vol. 205 (1991), pp.271-278,
15. G. A. Carpenter and S. Grossberg: ART2 : Self-Organization of Stable Category Recognition Codes for Analog Input Patterns, *Applied Optics,* Vol. 26, No. 23 (1987), pp.4919-4930
16. J. A. Freeman and D. M. Skapura: Neural Network: Algorithm, Applications and Programming Techniques, *Addison-Wesley Publishing Company Inc.,* (1991), pp.291-326
17. Y. H. Pao: Adaptive Pattern Recognition and Neural Networks, *Addison-Wesley Publishing Company Inc.,* (1989), pp.171-183